Local dynamic buckling of FPSO steel catenary riser by coupled time-domain simulations

T.S. Eom, M.H. Kim[*], Y.H. Bae and C. Cifuentes

Texas A&M University, College Station, Texas, USA

Abstract. Steel catenary riser (SCR) is a popular/economical solution for the oil/gas production in deep and ultra-deep water. The behavioral characteristics of SCR have a high correlation with the motion of floating production facility at its survival and operational environments. When large motions of surface floaters occur, such as FPSO in 100-yr storm case, they can cause unacceptable negative tension on SCR near TDZ (touch down zone) and the corresponding elastic deflection can be large due to local dynamic buckling. The generation, propagation, and decay of the elastic wave are also affected by SCR and seabed soil interaction effects. The temporary local dynamic buckling vanishes with the recovery of tension on SCR with the upheaval motion of surface floater. Unlike larger-scale, an-order-of-magnitude longer period global buckling driven by heat and pressure variations in subsea pipelines, the sub-critical local dynamic buckling of SCR is motion-driven and short cycled, which, however, can lead to permanent structural damage when the resulting stress is greatly amplified beyond the elastic limit. The phenomenon is extensively investigated in this paper by using the vessel-mooring-riser coupled dynamic analysis program. It is found that the moment of large downward heave motion at the farthest-horizontal-offset position is the most dangerous for the local dynamic buckling.

Keywords: vessel-mooring-riser coupled simulation; steel catenary riser (SCR); touch down zone (TDZ); sub-critical local dynamic buckling; 100-yr & 10-yr storm; riser-seabed interaction; elastic wave propagation/decay; turret-moored FPSO

1. Introduction

Floating Production Storage and Offloading (FPSO) is a combined design of storage and production/operation at remote development sites. It has been spotlighted as one of the most economic solutions for deepwater oil production without existing pipeline infrastructures and successfully installed and operated around the world for decades. Among various systems of position keeping for FPSO, the turret mooring systems enable FPSO to weather-vane around the turret to minimize environmental loads. SCR is a steel pipeline which hangs freely from the turret and gently curves down to the seabed. The motions of floating platform and SCR are coupled and the coupled responses affect the stress on SCR. Major concerns with the SCR design are structural failures associated with buckling or fatigue near the hang-off point or touchdown zone (TDZ).

When a floating platform experiences large motions in extreme environments, the connected

---

∗Corresponding author, Professor, E-mail: m-kim3@neo.tamu.edu

SCR may suffer compressional loading and the corresponding buckling-type deflections may occur near the touchdown point (TDP), where the mean tension is smaller than other parts of SCR. The buckling-type elastic waves generate large curvatures and bending moments, which may result in unallowable stress magnitude that leads to permanent damage. In the vessel-mooring-riser coupled dynamic analysis of this study, the bending moment spike can be observed where the local dynamic buckling occurs. Once the elastic waves are formed, their amplitudes grow until the tension is recovered from negative to positive values. Kuiper *et al*. (2007) simulated such local-dynamic-buckling phenomenon for a simple vertical riser connected to a floater undergoing large sinusoidal heave motion. He named this kind of instability of riser as sub-critical local dynamic buckling. In the present study, a much more complicated oil/gas production system, the turret-moored FPSO with numerous SCRs in two different hurricane conditions, will be investigated by using 3-hour time-domain simulation results.

The drastic increase of bending moment and stress beyond the elastically accepted level due to local dynamic buckling should be avoided in the design. To avoid the problem, a lazy-wave type geometry can artificially be introduced by adding many buoyancy units on the SCR but it is a much more expensive solution and can cause unfavorable flow-assurance problem (Jacob *et al*. 1999, Yue *et al*. 2010). Therefore, if the simple SCR is allowable for the given design environment, it is the simplest and least expensive solution.

Song and Stanton (2009) introduced the design procedure of SCR including major issues, related techniques, software, and regulations, fatigue assessment, and design confirmation. However, it did not include the fully-coupled time-domain simulation and scientific explanation of local dynamic buckling. As far as authors know, the direct and detailed simulation of temporary local dynamic buckling of SCR from a vessel-mooring-riser fully coupled program has not been published in the open literature. There are many references though about larger-scale an-order-of-magnitude-longer-period static-like buckling phenomena of submarine pipelines.

Seabed model normally consists of vertical stiffness and lateral/axial friction. Bruton *et al*. (2006, 2008) modeled the lateral pipe-soil interaction in a case study presenting the mechanism of long-term buckling in the lateral direction and heating/cooling-driven pipe walking in the axial direction on seabed. Zhou *et al*. (2010) introduced a similar long-term interaction between the pipe walking and lateral buckling on seabed in cyclic displacement. He defined the pipe walking as a global axial displacement driven by start-up/shut-down cycles of high thermal loading. Aubeny (2008, 2009) presented a seabed model with soil stiffness and backbone curve to simulate the penetration of SCR into the seafloor following the cycle of unloading and reloading using P-y curve. The seabed memory in his model is simulated as a trench at TDZ. However this kind of long-term soil deformation with memory effects and the corresponding long-term change of soil stiffness and friction are beyond the scope of this paper and no effort is made to include such long-term effects in the present numerical simulation.

2. Numerical models

2.1 Turret-moored FPSO system

As shown in Fig. 1, the numerical model of FPSO is a 200,000 DWT class crude oil tanker moored by the 12 mooring lines and connected to 13 SCRs through a single turret in 914-meter water depth. The particulars of the turret-moored FPSO and mooring lines are summarized in

Tables 1 and 2 (Wichers and Devlin 2001). In this study, the bending stiffness of the SCRs is based on Young's modulus of steel (78.5 kN/m) as shown in Table 4. The tangential drag and tangential added inertia are not considered in the program since they are negligible. The normal drag and normal added inertia coefficients for the present numerical model are shown in Table 3.
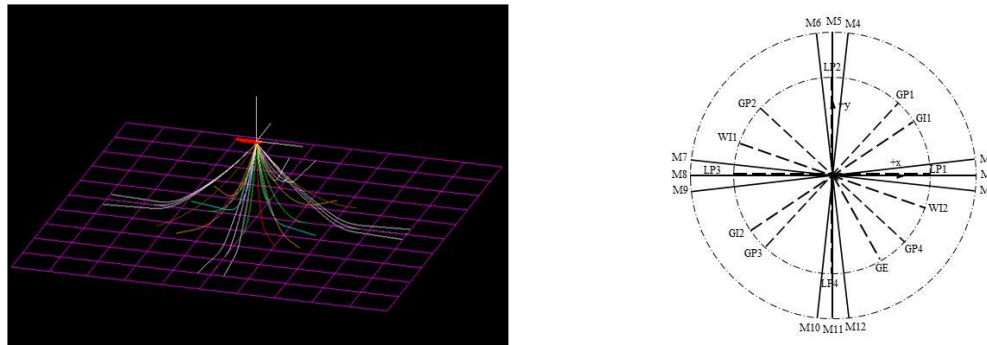

Fig. 1 Arrangement of mooring lines and SCRs

Table 1 Main particulars of FPSO (Wichers and Devlin 2001)

Description	Symbol	Unit	Value
Production level		*bpd*	120,000
Storage		*bbls*	1,440,000
Vessel size		*kDWT*	200.0
Length between perpendicular	Lpp	*m*	310.00
Breadth	B	*m*	47.17
Depth	H	*m*	28.04
Draft	T	*m*	18.9
Displacement		*MT*	240,869
Length-beam ratio	L/B		6.57
Beam-draft ratio	B/T		2.5
Block coefficient	Cb		0.85
Center of buoyancy Forward section10	FB	*m*	6.6
Center of gravity above Base	KG	*m*	13.3
Water plane area	A	m^2	13,400
Frontal wind area	Af	m^2	1011.7
Transverse wind area	Ab	m^2	3771.9
Roll radius of gyration at CG	R_{xx}	*m*	14.77
Pitch radius of gyration at CG	R_{yy}	*m*	77.47
Yaw radius of gyration CG	R_{zz}	*m*	79.30
Turret in center line behind Fpp (20.5% Lpp)	Xtur	*m*	63.55
Turret elevation below tanker base	Ztur	*m*	1.52
Turret Diameter		*m*	15.85

Table 2 Main particulars of mooring system (Wichers and Devlin 2001)

Designation	Unit	Value
Water depth	m	914
Pre-tension	kN	1201
Number of lines		4×3
Degree between the 3 lines	deg.	5
Length of mooring line	m	2,088
Segment 1(ground section): Chain		
Length at anchor point	m	914.4
Diameter	cm	8.89
Dry weight	N/m	1,617
Weight in water	N/m	1,407
Stiffness AE	kN	794,487
Mean breaking load (MBL)	kN	6,512
Segment 2: Spiral strand		
Length	m	1127.8
Diameter	cm	8.89
Dry weight	N/m	412.23
Weight in water	N/m	349.75
Stiffness AE	kN	689,858
Mean breaking load (MBL)	kN	6,418
Segment 3(FPSO section): Chain		
Length	m	45.7
Diameter	cm	8.89
Dry weight	N/m	1,617
Weight in water	N/m	1,407
Stiffness AE	kN	794,487
Mean breaking load (MBL)	kN	6,512

Table 3 Hydrodynamic coefficient of mooring lines

Hydrodynamic Coefficients	Symbol	Chain	Rope/Poly
Normal drag	C_{dn}	2.45	1.2
Normal added inertia coefficient	C_{in}	2.00	1.15

Table 4 Main particulars of risers (Revised LP line from Wichers and Devlin, 2001)

Riser type	Qt	OD	ID	AE	EI	Weight (dry/wet)	C_{dn}	Pre-tension
		m	*m*	*kN*	*$kN.m^2$*	*kg/m*		*kN*
Liquid production	4	0.254	0.208	3.34E+06	2.25E+04	134/99	1	1,112
Gas production	4	0.386	0.350	4.16E+06	7.06E+04	167/47	1	609
Water injection	2	0.531	0.495	5.80E+06	1.91E+05	286/193	1.414	2,019
Gas injection	2	0.287	0.247	3.36E+06	3.01E+04	185/119	1.414	1,352
Gas export	1	0.343	0.309	3.48E+06	4.64E+04	138/43	1	454
Each length					1,500 m			

2.2 Hull, mooring, SCR discretization

For the hydrodynamic calculations of the FPSO, hydrodynamic coefficients are calculated from frequency-domain 3D diffraction/radiation panel program (Lee *et al*. 1991). Then, they are used in the subsequent time-domain simulations based on Cumming's equation and two-term Volterra-series model. The hull motion is fully coupled with mooring and riser dynamics by solving the whole system in a combined matrix at each time step by using the computer program CHARM3D developed by the second author's research group during the past two decades (e.g., Kang and Kim 2012, Yang and Kim 2011, Tahar and Kim 2003). The half hull below mean water level is discretized by 1,831 quadrilateral panels after using geometric symmetry. Convergence tests were conducted before choosing the selected panel discretization. The viscous effects are also included through Morison's drag formula on each segment of the hulls to better estimate viscous loads. The second-order slowly varying wave loads are simulated by using the so-called Newman's approximation method. The reliability of the present numerical simulation of the FPSO system has been verified through many comparisons against experimental results (e.g., Tahar and Kim 2003, Kim *et al*. 2005). The mooring lines are modeled by 46-meterhigh-order members for each. In particular, the SCRs should be carefully discretized using appropriate size of mesh to minimize numerical errors. Particularly, fine-enough mesh is required near the touchdown zone (TDZ), along the seabed, and hang-off point, where the variations of force components are significant. If the element length is too long, it may suffer non-physical inner-element numerical instability under negative tension, which may occur for FPSO SCRs under severe storm conditions. In this study, homogeneous 12-meter high-order elements are used for the discretization of the target SCR, which is liquid production riser #1 (LP1) as shown in Figure 1. Its total length is 1,500 m, therefore 125 high-order elements are used for the target SCR.

The FE method is based on the formulation using rod element and generalized coordinate and thus more efficient than the typical FE program including coordinate transformation. The formulation includes extension and bending of the rod element but neglects twisting/torque and warping since their effects are negligible in mooring/riser global dynamics. The program first seeks a statically equilibrium position with the applied static components of environmental loadings and then starts time marching with the applied dynamic loads. The variations of the instantaneous moment arms due to rotational motions by mooring/riser tensions at connection points are incorporated in the algorithm to obtain more accurate instantaneous mooring/riser-induced moments. More details can be found from Koo and Kim (2005) and Yang and Kim (2011).
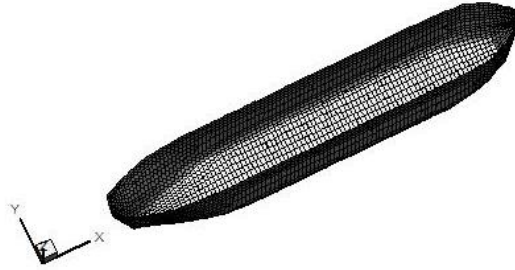
Fig. 2 Discretization of FPSO hull

2.3 Environmental condition

100-year- and 10-year- return-period hurricanes at the central area of the Gulf of Mexico are applied as the environmental condition in this study. The corresponding wave, current, and wind conditions are based on API 2INT-MET (2007) and they are tabulated in Table 5. The applied currents are storm induced steady shear currents. For simplicity, each environmental load is designed to be unidirectional and propagates to the same head direction. JONSWAP wave spectrum and API wind spectrum are used to generate the long-crested irregular random waves and dynamic wind velocities, respectively. The target and generated JONSWAP spectra and the generated wind-load time series are shown in Fig. 3 and 4, respectively.
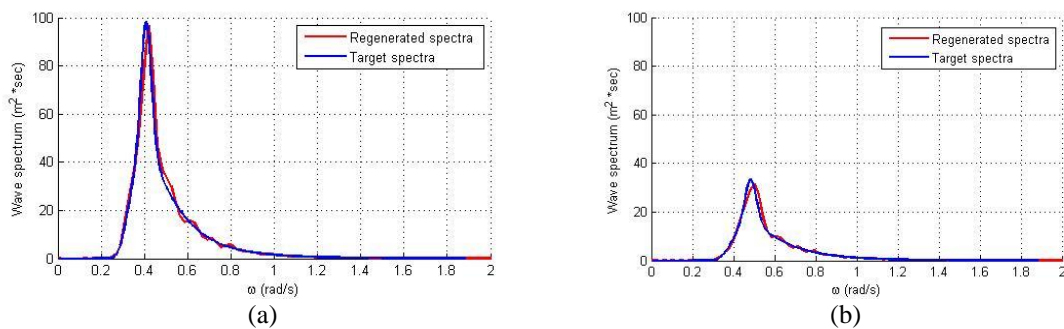
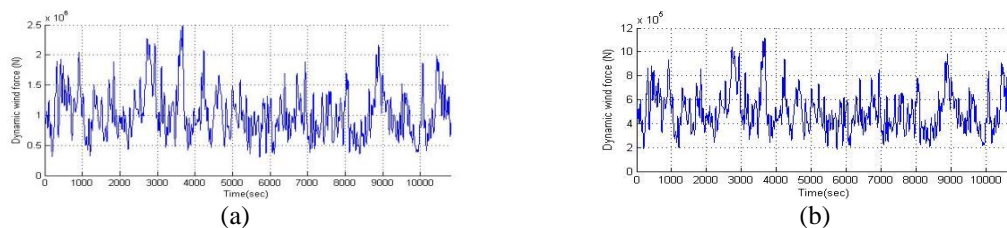Fig. 3 JONSWAP wave spectra at the central GOM; (a) 100-year hurricane, (b) 10-year storm

Fig. 4 Wind-loadtime series; (a) 100-year hurricane and (b) 10-year storm

Table 5 Environmental condition

Return Period	100 year		10 year	
Hs (m)	15.80		10.0	
Tp (sec)	15.40		13.0	
γ	2.4		2.4	
1-hour Mean Wind Speed (m/sec)	48.01		33.0	
	Depth (m)	Speed (m/sec)	Depth (m)	Speed (m/sec)
	0.0	2.41	0.0	1.65
Current Profile	50.4	1.80	34.7	1.24
	100.8	0	69.3	0
	914.0	0	914.0	0

2.4 Seabed-interaction modeling

In this study, the seabed is modeled as elastic flat surface using vertical stiffness and longitudinal/lateral friction. Continuous quadratic-spring foundation is used for the seabed stiffness model, while coulomb friction ($\mu \cdot F_{downward}$ where μ=friction coefficient) is used for the simulation of soil friction in the horizontal direction (see Fig. 5). In calculating the downward local net weight (weight minus buoyancy), it was compensated by instantaneous inertia loading in that direction. One of the advantages of the quadratic-spring foundation over the linear-spring foundation is that using the quadratic-spring foundation, it can better simulate the hardening of soil with penetration of pipeline to the seabed than the linear-spring foundation. However, local seabed deformation/slope and soil memory, such long-term effects as trench (downward) and berms (lateral) both formed by interaction of SCR and seabed especially near touchdown zone (TDZ),are not considered. Therefore, the seabed-friction model in this study is designed as a flat floor with constant friction as shown in Fig. 5. The applied seabed stiffness and friction coefficient are1E+07 (N/m^2) and 0.5, respectively. When necessary, the additional lateral linar damping proportional to the pipe lateral velocity can be inputted.

2.5 Local bending moment

The calculated local bending moments by the applied FE program are double-checked by the analytical formula. The variation of the bending moment near the TDZ is typically very rapid, and thus this kind of re-check is necessary particularly associated with the possible local dynamic buckling. In case of linearized beam theory, the bending moment of the plane section beam is the product of bending stiffness EI and the curvature k (=1/R) of the beam. The curvature can be calculated from the instantaneous-displacement data of the SCR nodes (Figs. 6 and 7).
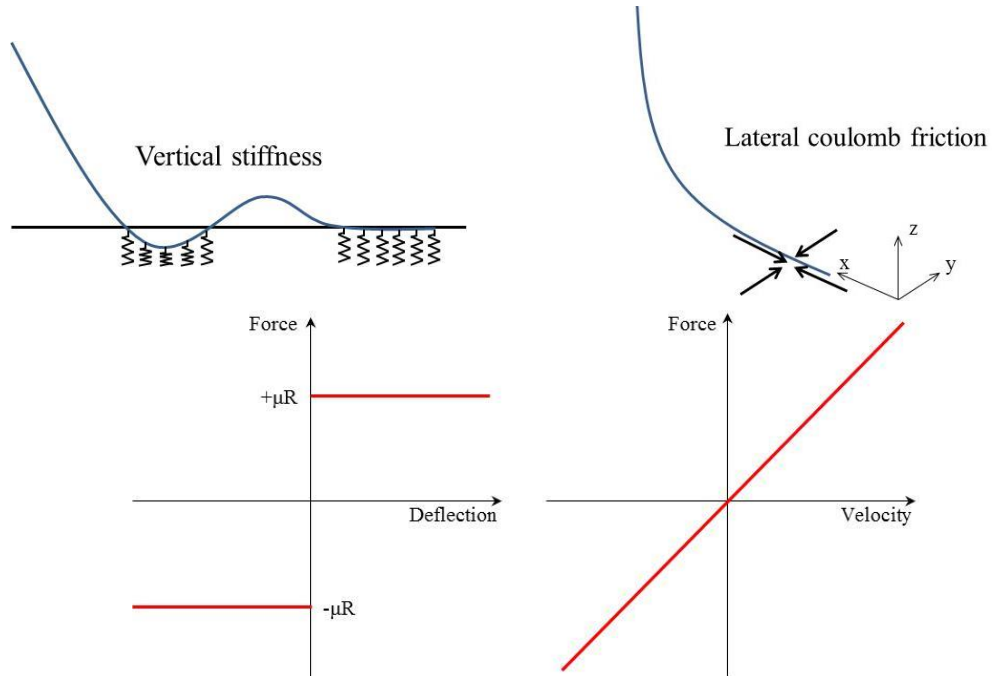
Vertical stiffness

Lateral coulomb friction

Force

+μR

Deflection

-μR

Force

Velocity

Fig. 5 Seabed spring/friction/damping model
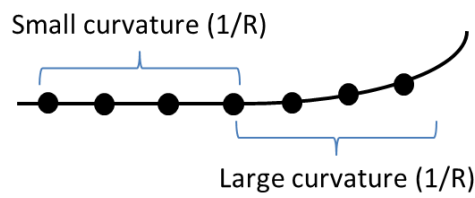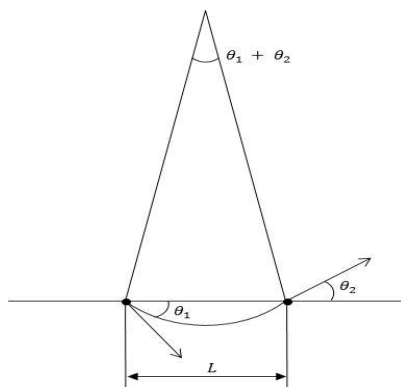
Small curvature (1/R)

Large curvature (1/R)

Fig. 6 Curvature of SCR

$$L = \left[? \ R^2 - 2R^2 \cos\left(\theta_1 + \theta_2\right) \right]^{1/2}$$

$$R = \frac{L}{\left[2 - 2\cos\left(\theta_1 + \theta_2\right) \right]^{1/2}}$$

$$BM = EI / R$$

Fig. 7 Curvature of an element

3. Time series analysis

Time-domain simulations of FPSO, SCRs, and mooring lines are performed using CHARM3D. The 6 degree-of-freedom (DOF) motions of FPSO are the dominant driving factor of the behavioral characteristics of SCRs, and therefore, each 6 DOF motions are firstly analyzed in time series. The corresponding coupled variations of tension and bending moment on SCR are also obtained. Particularly, 6 nodes are selected near TDZ for more detailed observation. The rough configuration of the 6 nodes on the target SCR including the coordinate system is shown in Fig. 8.
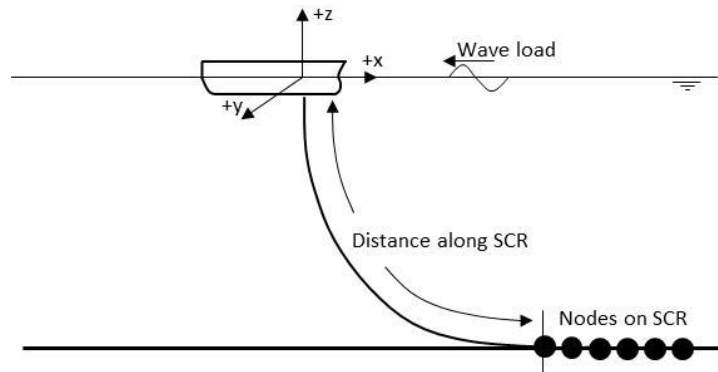
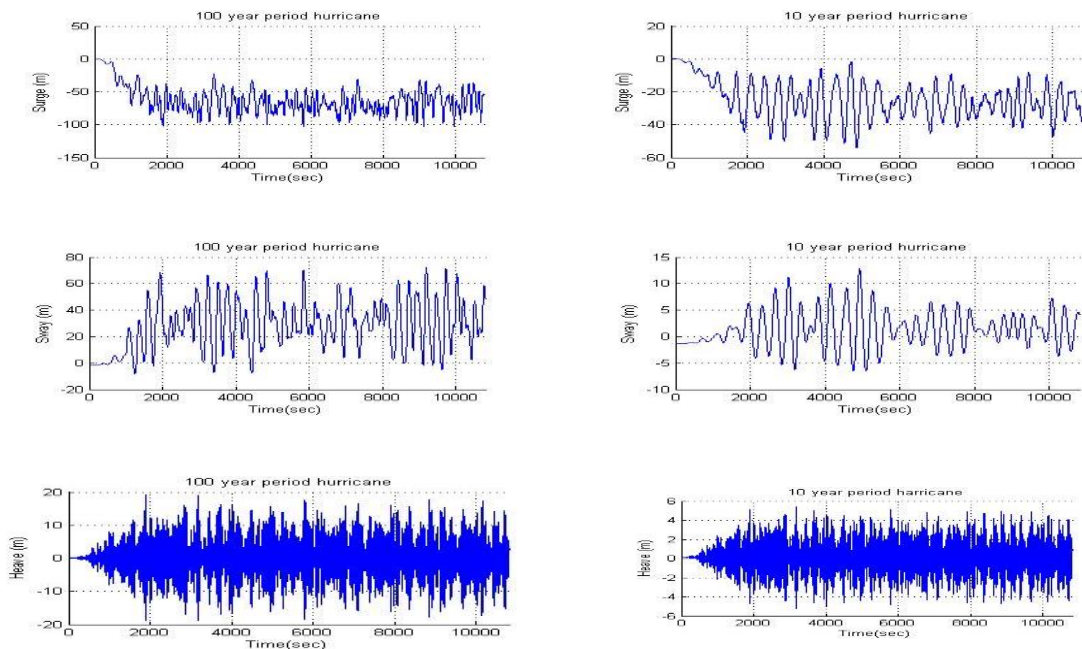Fig. 8 SCR configuration and 6 target points near TDZ

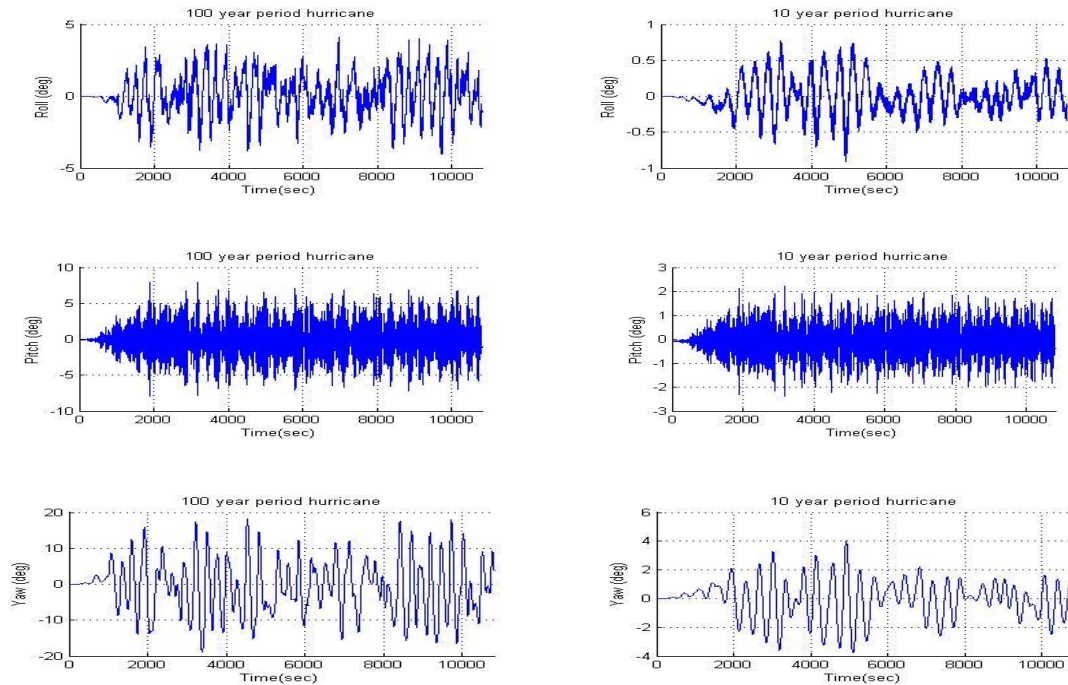Fig. 9 Time series of the translational motions of FPSO

Fig. 10 Time series of the rotational motions of FPSO

In Figs. 9 and 10, the motion time histories of FPSO in the given environmental condition are plotted. Among the translational motions, heave has the largest frequency, which leads to large velocity in the heave direction. In case of turret-moored FPSO, the pitch motions can also appreciably contribute to the downward motion at the turret position, to which SCRs are connected. This effect is larger, if the turret position is farther away from the mid-section. The vertical-plane motions (heave-pitch) are dominated by wave-frequency motions, while horizontal-plane motions (surge-sway-yaw) are dominated by slowly-varying motions, which is typical to slack-moored system. The horizontal mean offset and other dynamic motion amplitudes are significantly reduced in the 10-yr hurricane condition, which results in much less concern for the SCR design.

The motions of SCR near TDZ are shown in Figs. 11-13. The results for 100-year and 10-year hurricanes are shown in parallel in those plots. It needs to be remembered that the TDP is not fixed, instead continuously moving depending on the vessel position. There is also a big curvature change near TDZ from the near-vertical to the near-horizontal (on seabed) and a possibility of bottom-touching impact loads. Therefore, this is the most critical portion of SCR in the design from the point of maximum stress and fatigue failure. The displacements in two different environmental conditions show significant differences in magnitude and the behavior of SCR on the seabed. The x-directional riser displacements mean that they are lateral motions above the TDZ and axial motions for that on seabed. Therefore, there is a big change in magnitude. The y-directional riser displacements are mostly influenced by sway and yaw vessel motions and they are significantly reduced when the riser is laid on seabed due to the bottom-friction effect. The z-directional riser displacements are mostly influenced by heave and pitch vessel motions and they are rapidly reduced after TDZ since the portion is laid on seabed. The 10-yr case has the same

pattern with much reduced amplitude. As for the top portion of the riser, their mean tension is large and they move with almost the same acceleration, so no negative tension happens. However, for the portion near TDZ, there is a big change in vertical acceleration (whose magnitude is roughly vertical displacement multiplied by circular frequency squared), and in the case of downward motion, significant negative tension may occur due to compressional inertia loading combined with larger drag on lower portion, which may lead to local dynamic buckling there.

The time series of tensions and bending moments on the corresponding spots of SCR near TDZ are also displayed in Figs. 14 and 15 in the same manner. Fig. 14 shows that negative tensions (compressional load) occur along all spots of the portion and their magnitudes are similar in case of 100-yr hurricane. For 10-yr hurricane case, dynamic tensions are small and there is no sign of negative tension. Fig. 14 shows the corresponding time series for local bending moment and its magnitude can increase a lot due to temporary local dynamic buckling caused by temporary compressional loading. If it happens within elastic limit, it can go back to the original shape, but otherwise, its damage can remain or lead to structural failure. Therefore, this should be the most serious factor in the design of FPSO-SCR in harsh environment. We do not see that kind of phenomenon in 10-yr hurricane. This is why FPSO-SCR is popular in more benign environments, such as West Africa but not popular in the hurricane-prone regions, such as GOM. Tables 6-12 contain the corresponding statistics data of Figs. 9-15.The comparison of the mean and standard deviation of FPSO motions between the 100-year and 10-year hurricanes features that the hull dynamics in the 100-year hurricane is considerably larger than that of 10-year hurricane, which is in turn directly linked to the SCR dynamics and the corresponding risks.

Table 6 Statistics of FPSO-motion time series (excluding initial 1,000 sec in time series)

	100-year period hurricane				10-year period hurricane			
	Max	Min	Mean	STD	Max	Min	Mean	STD
Surge (m)	-22.8202	-103.1428	-66.2326	15.2428	-1.6687	-54.0631	-26.5244	10.2743
Sway (m)	72.1462	-8.2823	30.4571	17.8533	12.7781	-6.5444	1.5348	3.5431
Heave (m)	19.2310	-18.8986	0.0671	6.2054	5.3806	-5.1901	0.1056	1.7448
Roll (deg)	4.1014	-4.0072	0.1311	1.4622	0.7672	-0.9083	0.0061	0.2519
Pitch (deg)	7.9609	-7.9729	0.0581	2.5032	2.2253	-2.3735	-0.0754	0.6969
Yaw (deg)	18.1133	-18.8562	-0.8085	7.9232	4.0060	-3.7780	-0.0380	1.4258

Table 7 Statistics of time series on the node at 1,356 m from hang-off point(excluding initial 1,000 sec in time series)

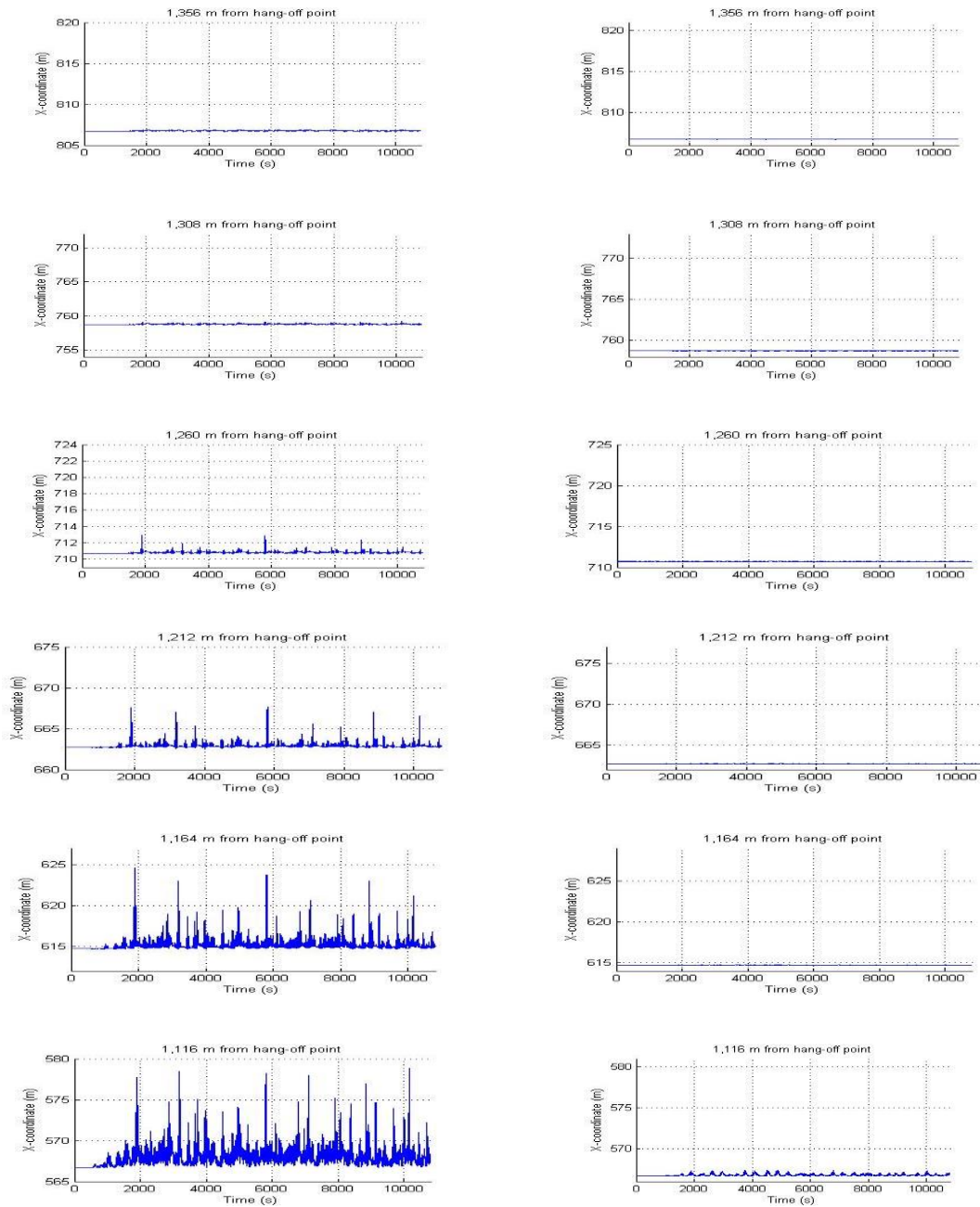|	100-year period hurricane		10-year period hurricane	
	Mean	STD	Mean	STD
X-dir coordinate (m)	806.7723	0.0369	806.7213	0.0022
Y-dir coordinate (m)	3.5826	1.2355	0.2498	0.1936
Z-dir coordinate (m)	-913.981	0.2469	-914.01	0.0019
Tension (N)	4.04E+05	4.76E+05	2.96E+05	5.71E+04
Bending moment (N-m)	1.96E+04	1.18E+04	2.13E+04	1.02E+04

Fig. 11 X-directional displacements of nodes over SCR near TDZ: (Left) in 100-year period hurricane, (Right) in 10-year period hurricane
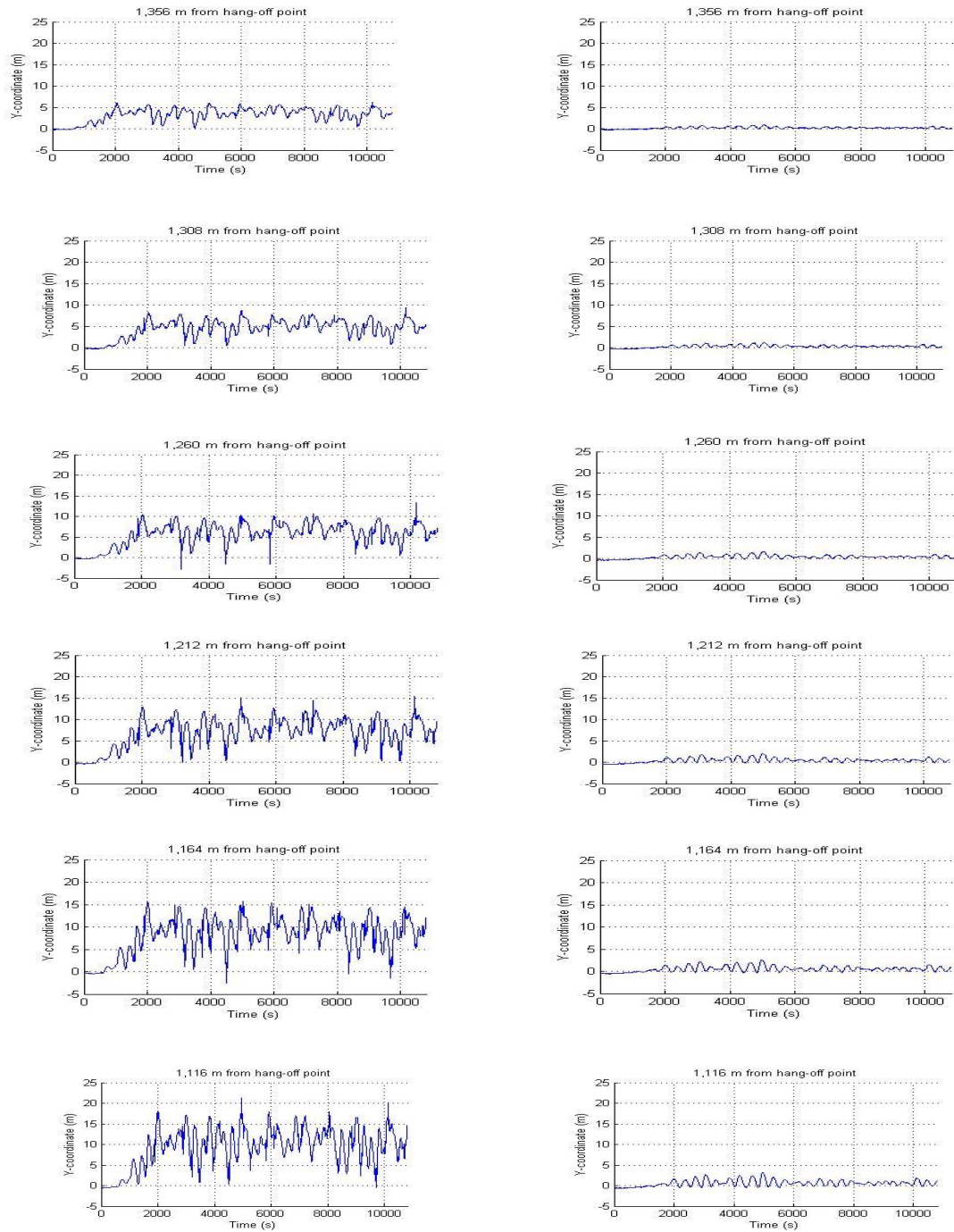
Fig. 12 Y-directional displacements of nodes over SCR at TDZ: (Left) in 100-year period hurricane, (Right) in 10-year period hurricane
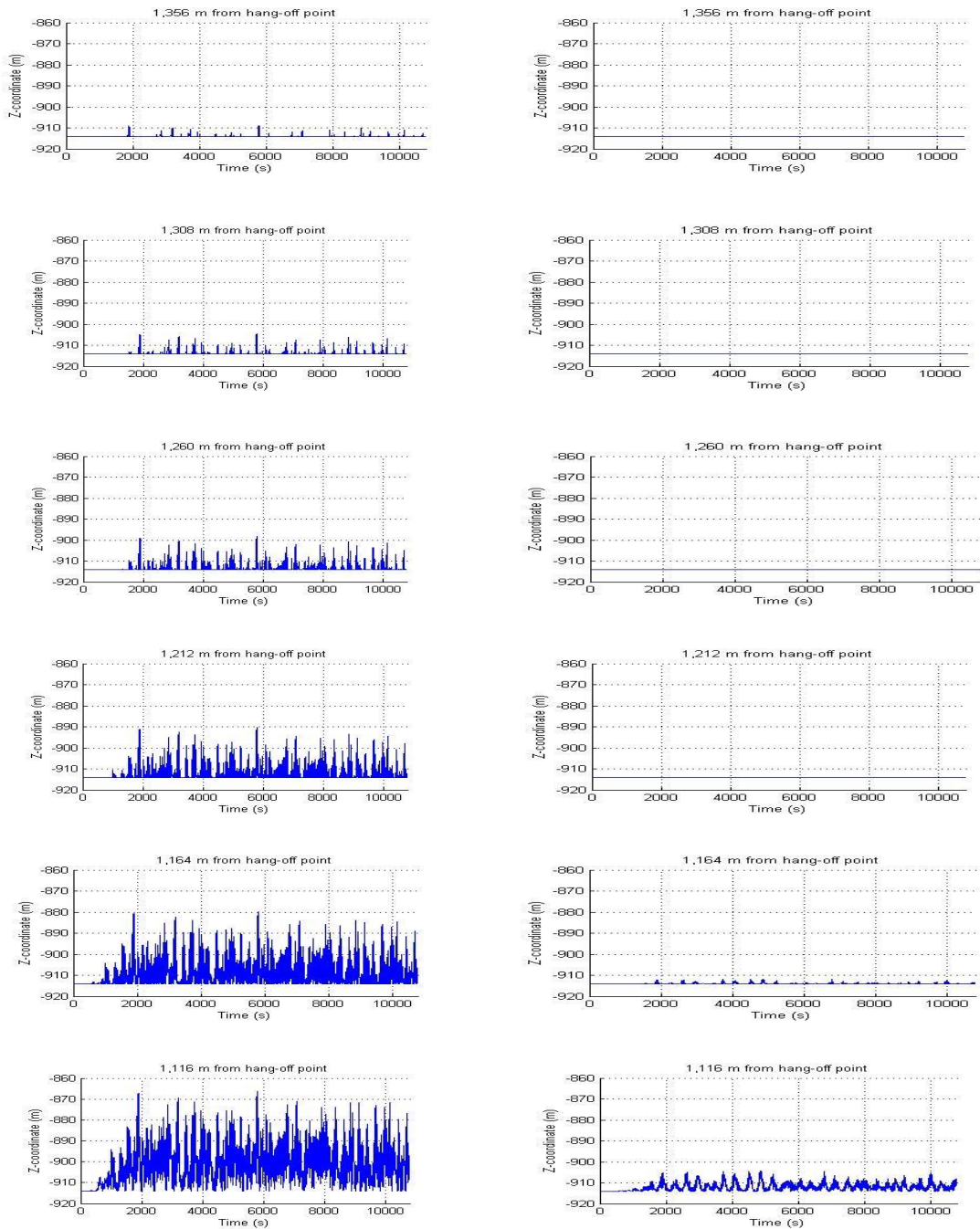
Fig. 13 Z-directional displacements of nodes over SCR at TDZ: (Left) in 100-year period hurricane, (Right) in 10-year period hurricane
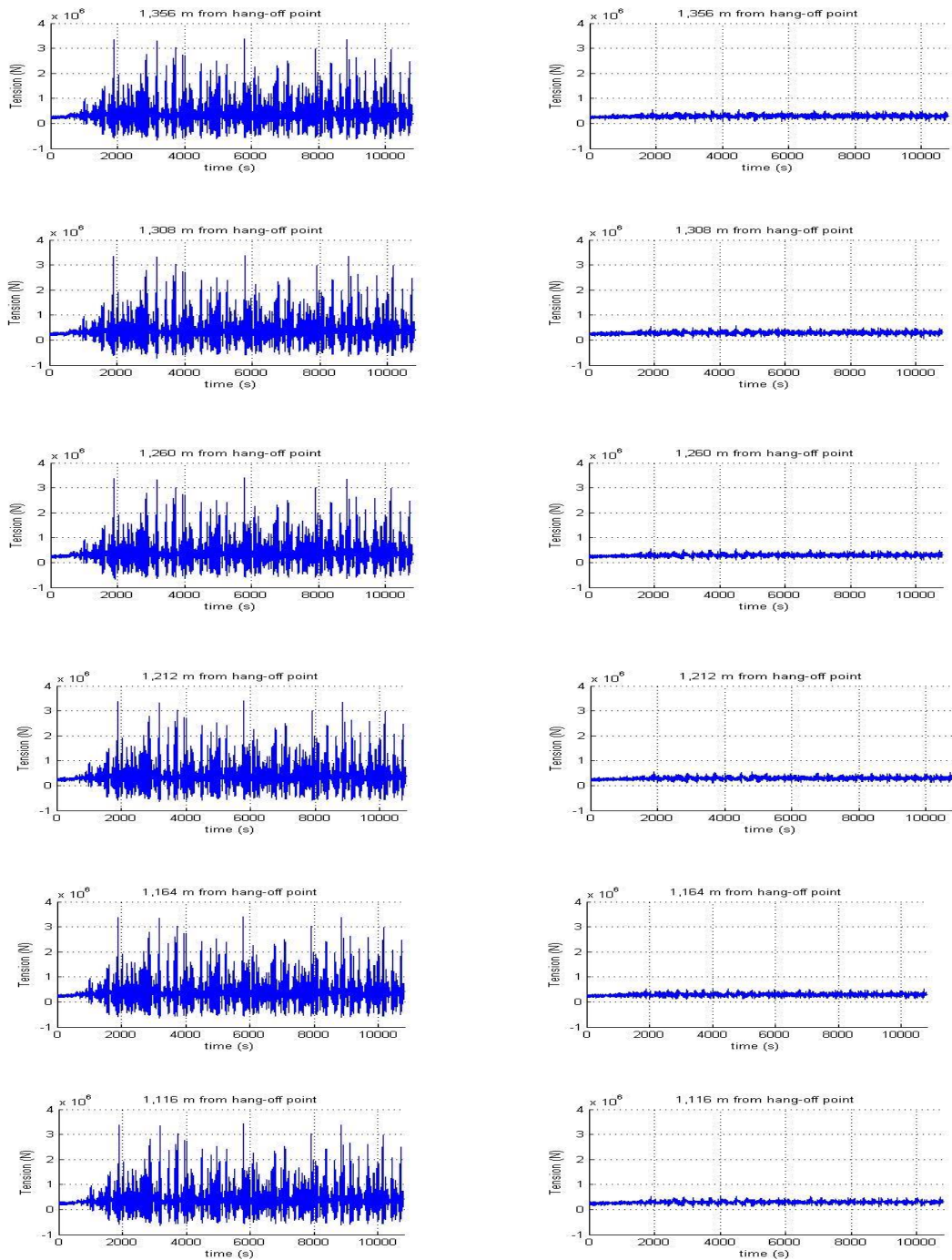
Fig. 14 Tensions at nodes over SCR at TDZ: (Left) 100-year period hurricane, (Right) 10-yr period hurricane
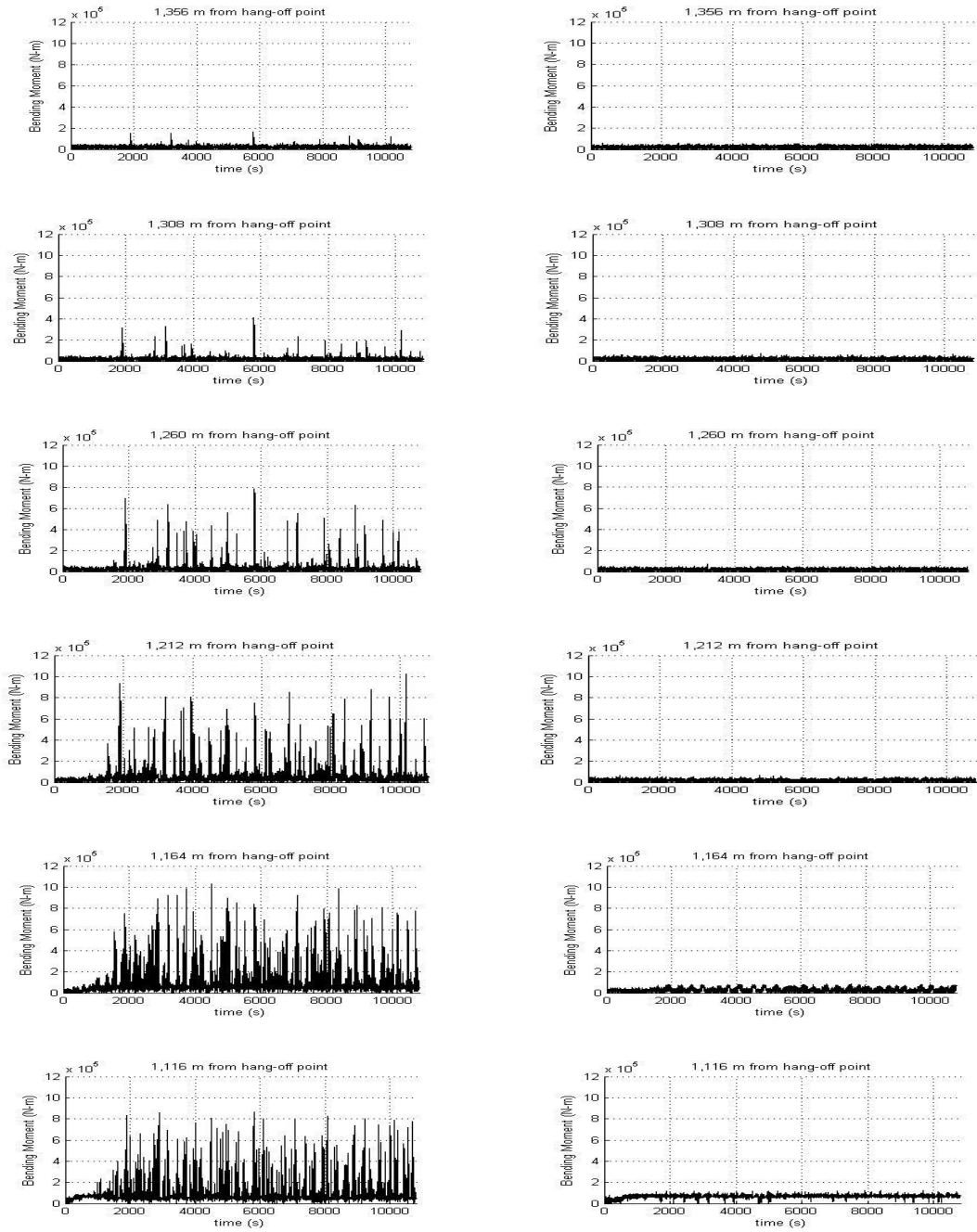
Fig. 15 Bending moment at nodes over SCR at TDZ: (Left) 100-year period hurricane, (Right) 10-year period hurricane
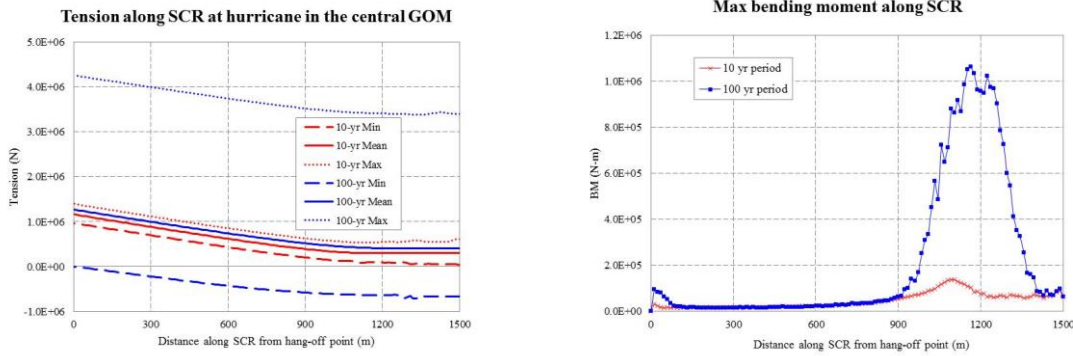
Fig. 16 Max-Mean-Minimum tension and Maximum bending moment on SCR

Fig. 16 shows max-min and mean tensions and maximum bending moments along the length-direction of the SCR. It is seen that the negative tension does not occur on any portion of the riser in 10-yr storm case. However, in the 100-yr storm case, almost all portions have negative tensions and their magnitudes grow toward the TDZ and then remain almost constant after that. As a result, local dynamic buckling may occur if the compressional loading reaches a critical value and then the bending moment can temporarily increase drastically, as shown in Fig. 16. If the resulting stress reaches the yielding point of a material, structural failure happens. In case of 10-yr storm case, no local dynamic buckling occurs and the corresponding increase of bending moment is very mild near the TDZ, as shown in the figure.

Table 8 Statistics of time series on the node at 1,308 m from hang-off point(excluding initial 1,000 sec in time series)

	100-year period hurricane		10-year period hurricane	
	Mean	STD	Mean	STD
X-dir coordinate (m)	758.7903	0.0547	758.7165	0.0029
Y-dir coordinate (m)	4.9018	1.6832	0.3422	0.2675
Z-dir coordinate (m)	-913.875	0.6835	-914.01	0.0017
Tension (N)	4.04E+05	4.76E+05	2.96E+05	5.57E+04
Bending moment (N-m)	2.09E+04	2.00E+04	1.89E+04	9.74E+03

Table 9 Statistics of time series on the node at 1,260 m from hang-off point(excluding initial 1,000 sec in time series)

	100-year period hurricane		10-year period hurricane	
	Mean	STD	Mean	STD
X-dir coordinate (m)	710.8265	0.126	710.7116	0.0037
Y-dir coordinate (m)	6.2451	2.1434	0.4354	0.3472
Z-dir coordinate (m)	-913.482	1.6332	-914.01	0.0017
Tension (N)	4.05E+05	4.77E+05	2.97E+05	5.45E+04
Bending moment (N-m)	2.80E+04	4.61E+04	1.96E+04	9.32E+03

Table 10 Statistics of time series on the node at 1,212 m from hang-off point(excluding initial 1,000 sec in time series)

	100-year period hurricane		10-year period hurricane	
	Mean	STD	Mean	STD
X-dir coordinate (m)	662.935	0.3504	662.7069	0.0045
Y-dir coordinate (m)	7.6147	2.6148	0.5296	0.4395
Z-dir coordinate (m)	-912.161	3.4308	-914.01	0.0018
Tension (N)	4.05E+05	4.78E+05	2.96E+05	5.50E+04
Bending moment (N-m)	4.54E+04	7.59E+04	1.83E+04	9.07E+03

Table 11 Statistics of time series on the node at 1,164 m from hang-off point (excluding initial 1,000 sec in time series)

	100-year period hurricane		10-year period hurricane	
	Mean	STD	Mean	STD
X-dir coordinate (m)	615.2951	0.7534	614.7035	0.0064
Y-dir coordinate (m)	8.9912	3.1194	0.622	0.5541
Z-dir coordinate (m)	-908.248	6.0842	-913.94	0.2236
Tension (N)	4.09E+05	4.78E+05	2.96E+05	5.58E+04
Bending moment (N-m)	7.23E+04	1.02E+05	2.81E+04	1.77E+04

Table 12 Statistics of time series on the node at 1,116 m from hang-off point (excluding initial 1,000 sec in time series)

	100-year period hurricane		10-year period hurricane	
	Mean	STD	Mean	STD
X-dir coordinate (m)	568.3257	1.2794	566.797	0.1135
Y-dir coordinate (m)	10.3511	3.6754	0.7009	0.6975
Z-dir coordinate (m)	-899.573	8.4942	-911.841	1.8269
Tension (N)	4.17E+05	4.77E+05	2.98E+05	5.18E+04
Bending moment (N-m)	7.56E+04	9.13E+04	6.89E+04	1.25E+04

Further insights on local dynamic buckling

As far as authors know, the direct and detailed simulation of temporary local dynamic buckling of SCR from a vessel-mooring-riser fully coupled program has not been published in the open literature. Actually, even the local dynamic buckling of a simpler system, such as vertical riser, has been very rare (e.g., Kuiper *et al*. 2007). There are many references though about larger-scale an-order-of-magnitude-longer-period static-like buckling phenomena of submarine pipelines. Therefore, let us focus more on the details of this phenomenon in the following.

Correlation of FPSO motion and force on SCR

Cheng et al (2007) introduced the correlation between the heave velocity at hang-off point and the tension on SCR at TDZ. The time series of the tension and hang-off heave velocity presented in Fig. 17 actually show high correlation to each other. The negative tension occurs during the downward heave motion at the turret position. If the downward heave motion is small, negative tension does not occur. The correlation between the heave velocity at hang-off point and the bending moment on SCR at TDZ is more complex than that of tension since the bending moment is also related to the local curvature and vessel-horizontal-offset positions. Figs. 18 and 19 illustrate the relation of FPSO motions (heave and surge) to the bending moment on SCR at TDZ. It is seen that the maximum bending moment is likely to occur for downward heave motions at maximum negative surge-offset positions.
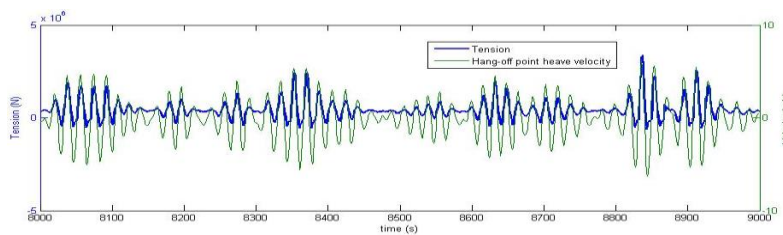

Fig. 17 Tension at TDZ and heave velocity at hang-off point in time series
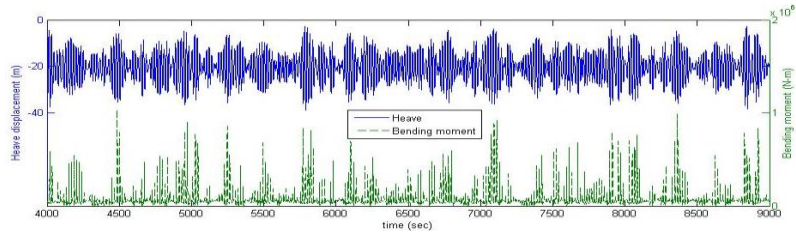
Fig. 18 Bending moment at TDZ and heave displacement at hang-off point in time series
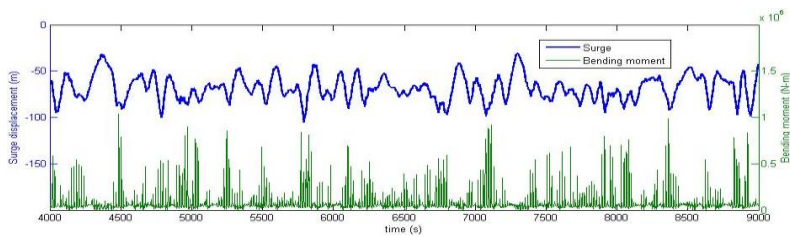

Fig. 19 Bending moment at TDZ and surge displacement at hang-off point in time series

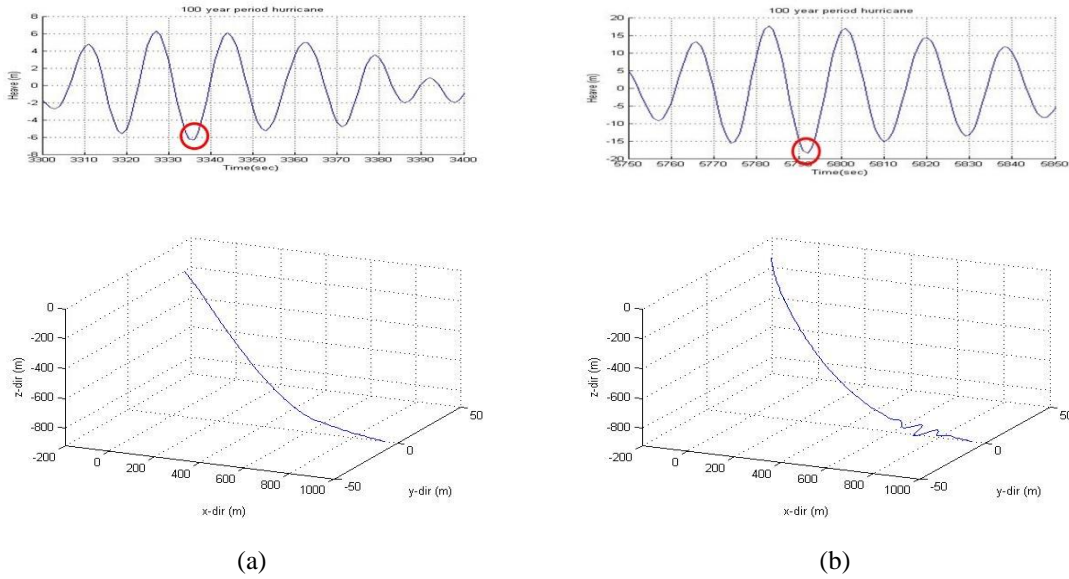(a)   (b)

Fig. 20 Snapshots of SCR; (a) at nearest vessel position from TDZ (3,335sec in time series), (b) at farthest
        vessel position from TDZ (5,792 sec in time series)

Fig. 20 also shows that the downward heave motions should be large enough to cause local dynamic buckling. There is no local dynamic buckling at the nearest horizontal offset position from the TDZ, while local dynamic buckling happens at the farthest horizontal offset position from the TDZ.

(a)   (b)
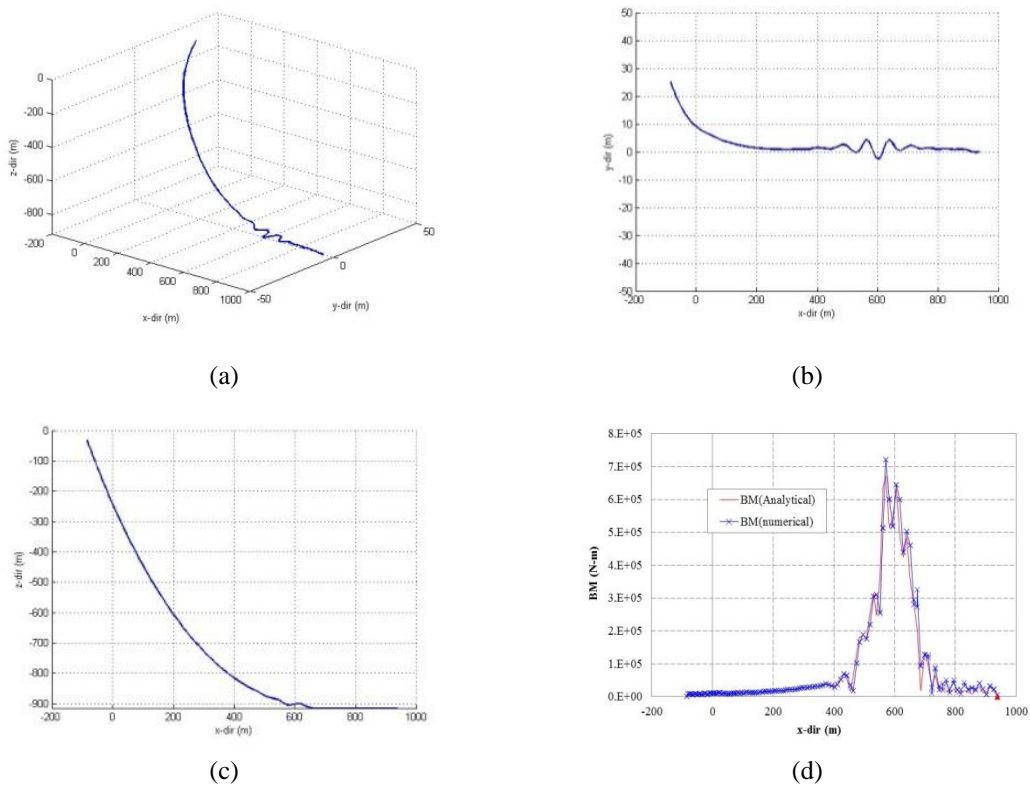

(c)   (d)

Fig. 21 Sub-critical local dynamic buckling: (a) XYZ plan, (b) XY plan, (c) YZ plan, (d) Bending moment

Fig. 21 shows the local dynamic buckling viewed from three different directions. The elastic waves have both vertical and lateral components. On the seabed, only lateral waves are noticeable. The numerically calculated bending moments are also checked by the analytical approach introduced earlier (Fig. 7) and they agree very well as shown in the Fig. 21(d).

More thoughts on local dynamic buckling

As was seen in the previous figures, the local dynamic buckling temporarily occurs near TDZ, where the pre-tension is smaller than other upper parts of SCR. It perishes when the hang-off point moves upward with the corresponding motion of FPSO. Therefore, the elastic waves generated by the instantaneous local dynamic buckling perish during that time and the deflections propagate farther away from that place. To see this phenomenon more clearly, let us consider a simpler case i.e., the simulation of harmonic oscillation of FPSO heave motion with 20-m amplitude and the corresponding dynamics of SCR near TDZ. The forced heave amplitude is large enough to periodically generate large negative tensions and local dynamic buckling near TDZ. A series of

snapshots of riser profiles during the local dynamic buckling are shown in Fig. 22. During the propagation period, the elastic wave amplitudes are decreased and the pulses are widened due to the damping and dispersion (see Fig. 22). When the frequency of this cycle is low enough to separate each buckling event from another, the buckling is called sub-critical local dynamic buckling. Kuiper *et al*. (2007) described and simulated this phenomenon by using the harmonic heave motion of floater with simple vertical top-tensioned risers and low drag coefficient.
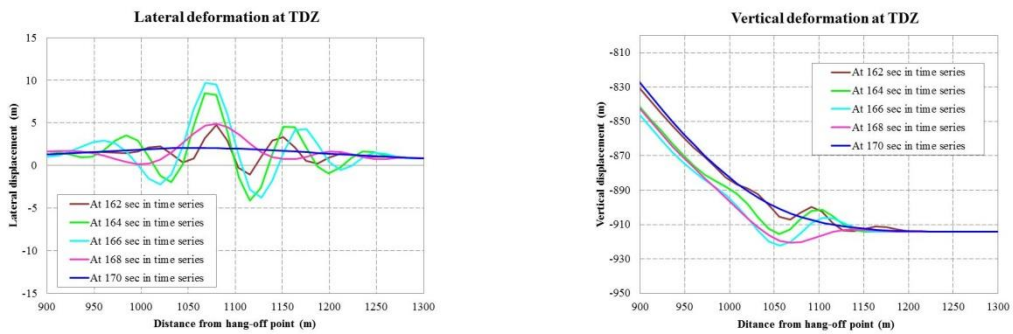

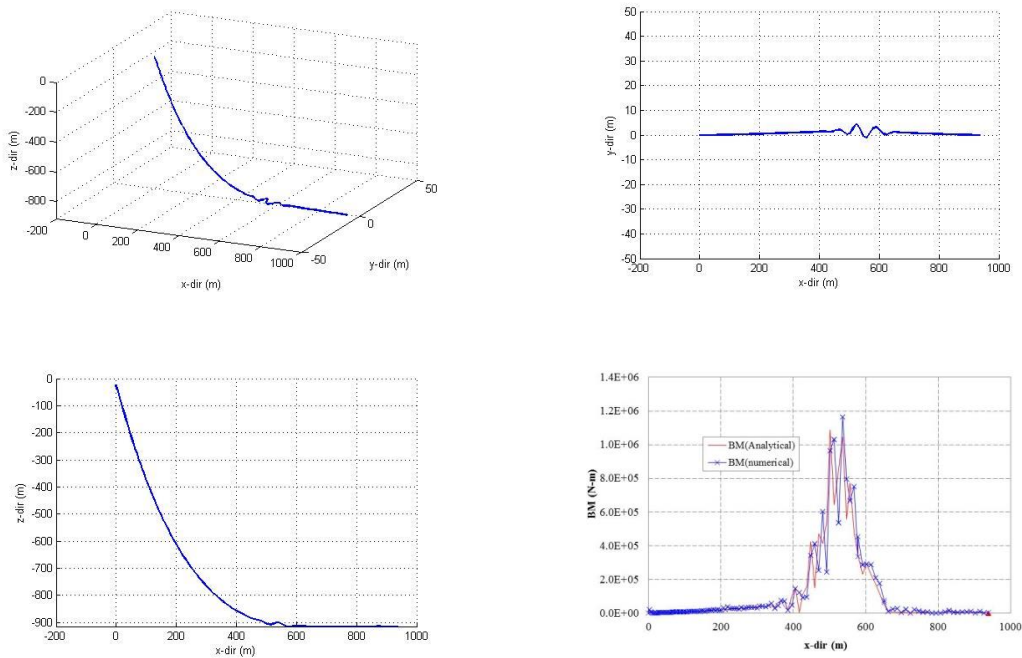Fig. 22 Successive shapes of Elastic waves generated by local dynamic buckling

Fig. 23 Sub-critical local dynamic buckling at 162 sec in time series: (a) XYZ plan, (b) XY plan, (c) YZ plan, (d) Bending moment
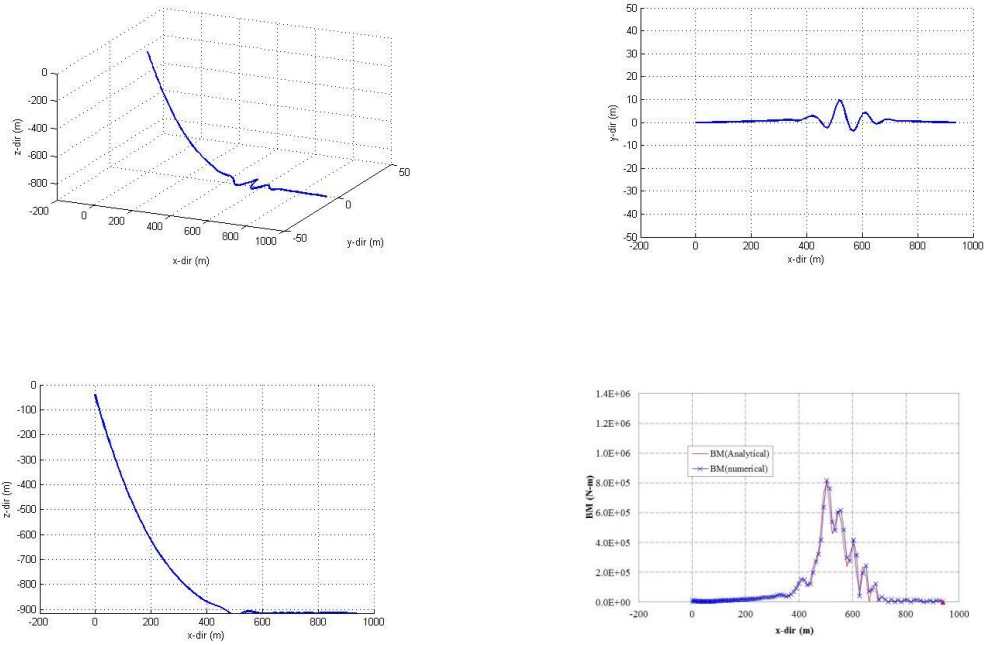
Fig. 24 Sub-critical local dynamic buckling at 166 sec in time series: (a) XYZ plan, (b) XY plan, (c) YZ plan, (d) Bending moment
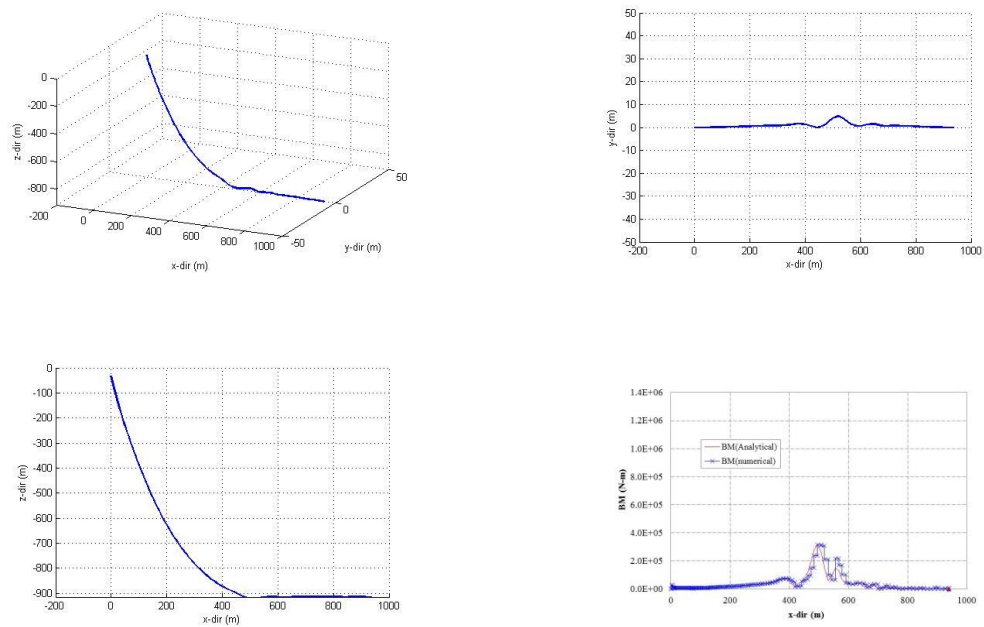

Fig. 25 Sub-critical local dynamic buckling at 168 sec in time series: (a) XYZ plan, (b) XY plan, (c) YZ plan, (d) Bending moment

Figs. 23-25 plot the detailed shapes of the SCR and the corresponding bending moment during the growth, maximum, and decay stages of local dynamic buckling. It is interesting that the maximum bending moment does not occur at the maximum buckling amplitude. Instead, it becomes very large during the initial growth stage (e.g., 162s). It is mainly due to the change of elastic-wave length (initially short wave length but it gradually increases with time). During the initial growth stage, even if the displacement amplitude is small, the corresponding wave length is also small, which results in larger curvature compared to other stages.

Comparison against McCann's simple formula

McCann (2003) introduced a simple criterion to roughly check whether the buckling of SCR may occur or not by using the ratio of hang-off velocity and terminal velocity. Terminal velocity is obtained when the drag force is balanced by the net downward gravity force. The vertical velocity of the upper portion of the SCR is close to that of hang-off heave velocity since the position is near vertical and the tangential frictional drag is small. However, when its curvature is changed from near-vertical to near-horizontal near TDZ, the relatively large cross-flow drag happens and the velocity of the element of SCR reaches near-steady terminal velocity. Therefore, we have large downward acceleration acting on the upper end, while zero acceleration at the lower end. Then, the large differences in vertical accelerations may generate local compressional loading near the TDZ. Therefore, the ratio of hang-off velocity and terminal velocity can in some sense be used as a measure of the occurrence of local dynamic buckling. Assuming unit length, the equation for the terminal velocity is as follows

$$F_{net} = m \cdot g - C_d \cdot \rho \cdot D_{drag} \cdot V_{Terminal}^{2} / 2 = 0$$

$$V_{Terminal} = \sqrt{2 \cdot m \cdot g / C_d \cdot \rho \cdot D_{drag}}$$

Where $m\,g$ = net weight per unit length, C_d = normal drag coefficient, D_{drag} = Drag Diameter, ρ = Water density, $V_{Terminal}$ = Terminal velocity

According to McCann's suggestion, if the ratio of heave hang-off velocity to the terminal velocity is greater than 1, buckling is likely to occur. By using the above equation and $C_d = 1$, the estimated ratio is greater than 2 in case of 100-yr storm (Fig. 26), which means that buckling will happen, which is actually the case. In the 10-yr-storm case (Fig. 27), The same estimation leads to the ratio less than 1, which means that buckling does not occur, which is actually the case. Therefore, the simple criterion is actually useful in roughly predicting the possibility of buckling in the absence of other reliable numerical tools.
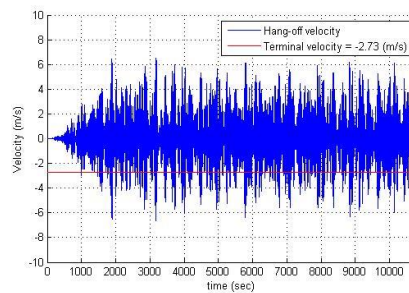

Fig. 26 Partial time series of hang-off heave velocity and terminal velocity
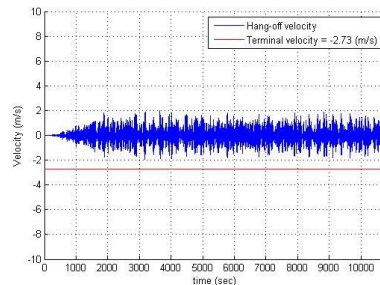
Fig. 27 Partial time series of hang-off heave velocity and terminal velocity

Double-checking with commercial software

For the verification of the present numerical simulations especially for the occurrence of local dynamic buckling, the same system was also simulated by another commercial program OrcaFlex (not fully-coupled simulation between vessel and mooring/riser). For this comparison, the prescribed harmonic heave oscillation of FPSO (same case as Fig. 22) was used for simplicity and the corresponding dynamic responses of the target SCR were compared. In both cases, the local dynamic buckling occurs at around the same spot with similar response pattern. The phenomenon occurs only for a short period in both cases and the generated elastic waves propagate away in a similar pattern. One main difference between the two results is that the vertical displacement of riser for the present model has somewhat larger value than that of OrcaFlex. This can be anticipated by using different seabed interaction model and stiffness in each program (e.g., present seabed-interaction model adopted quadratic spring model, while Orca Flex uses only linear spring model).

4. Conclusions

Sub-critical local dynamic buckling of SCR was analyzed by using the fully-coupled hull-riser-mooring dynamic analysis program. The coupled motions between FPSO and SCR were analyzed and the correlations between the motion of FPSO and the dynamic characteristics of SCR near TDZ were observed utilizing the corresponding time series. The cycle of the local dynamic buckling consists of growth and decay half-cycle. During the growth half-cycle, the corresponding bending moment can be significantly amplified near TDZ to pose a risk of permanent structural damage. If the instantaneous resultant stress (bending stress combined with other stresses) remains smaller than the elastic limit of the material, the local dynamic buckling does not cause any risk. The local dynamic buckling of SCR happens only when the vessel vertical (heave-pitch) motions are very large. For example, it occurs for FPSO-SCR in 100-yr storm but does not occur in 10-yr storm. It is also found that the moment of downward heave motion at the farthest-horizontal-offset position is the most dangerous for the local dynamic buckling. The interaction model between the seabed and SCR also influences the propagation and decay of the generated elastic waves. The accuracy of the numerically calculated bending moment was checked through comparison with analytical method. The overall correctness of the results was double-checked by comparing with

the results from an independent commercial program (OrcaFlex) of similar capability. The reasonability of McCann's simple criterion for buckling was also checked by the present numerical simulations. In the present study, local seabed deformation/slope and soil memory effect, such as time varying trench (downward) and berms (lateral) are not considered and it will be the subject of future study.

Acknowledgments

References

API Bulletin 2INT-MET (2007), *Interim guidance on hurricane conditions in the Gulf of Mexico*, American Petroleum Institute, 3-5, Washington, DC.

API RP 2RD (2009), *Design of risers for floating production systems (FPSs) and tension-leg platforms (TLPs)*, American Petroleum Institute, 83, Washington, DC.

Aubeny, C. and Biscontin, G. (2008), "Interaction model for steel compliant riser on soft seabed", *Proceedings of the Offshore Technology Conference*, Houston, TX.

Aubeny, C. and Biscontin, G. (2009), "Seafloor-riser interaction model", *Int. J. Geomechanics*, **9**, 133-141.

Bruton, D., White, D., Carr, M. and Cheuk, C. (2008), "Pipe-soil interaction during lateral buckling and pipeline walking – The SAFEBUCK JIP", *Proceedings of the Offshore Technology Conference*, Houston, TX.

Bruton, D., White, D., Cheuk, C., Bolton, M. and Carr, M. (2006), "Pipe/Soil interaction behavior during lateral buckling, including large-amplitude cycle displacement tests by the Safebuck JIP", *Proceedings of the Offshore Technology Conference*, Houston, TX.

Cheng, Y., Song, R., Mekha, B., Torstrick, A. and Liu, H. (2007), "Compression assessment of deepwater steel catenary risers at touch down zone", *Proceedings of the Offshore Mechanics and Arctic Engineering*, San Diego, CA.

Jacob, BP, Reyes, MCT, Lima, BSLP, Torres, ALFL, Mourelle, MM, and Silva, RMC (1999). "Alternative configurations for steel catenary risers for turret moored FPSOs", *Proceedings of the 9th Int. Offshore and Polar Eng. Conf.*, Brest, ISOPE.

Kang, H.Y. and Kim, M.H. (2012), "Hydrodynamic interactions and coupled dynamics between a container ship and multiple mobile harbors", *Ocean Syst. Eng.*, **2**(3), 217-228.

Kim, M.H., Koo, B.J., Mercier, R.M. and Ward, E.G. (2005), "Vessel/mooring/riser coupled dynamic analysis of a turret-moored FPSO compared with OTRC experiment", *Ocean Eng.*, **32**, 1780-1802.

Koo, B.J. and Kim, M.H. (2005), "Hydrodynamic interactions and relative motions of two floating platforms with mooring lines in side-by-side offloading operation", *Appl. Ocean Res.*, **27**(6), 295-310.

Kuiper, G., Brugmans, J. and Metrikine, A. (2007), "Destabilization of deep-water risers by a heaving platform", *J. Sound Vib.*, **310**, 541-557.

McCann, D., Smith, F. and O'Brien, P. (2003), "Guidelines for compression modeling in flexible risers for deepwater applications", *Proceedings of the Offshore Technology Conference*, Houston, TX.

Song, R. and Stanton, P. (2009), "Advances in deepwater steel catenary riser technology state-of-the-art: part II – Analysis", *Proceedings of the Offshore Mechanics and Arctic Engineering*, Hawaii, USA

Tahar, A. and Kim, M. (2003), "Hull/mooring/riser coupled dynamic analysis and sensitivity study of a tanker-based FPSO", *Appl. Ocean Res.*, **25**(6), 367-382.

Wichers, J.E.W. and Devlin, P.V. (2001), "Effect of coupling of mooring lines and risers on the design values for a turret moored FPSO in deep water of Gulf of Mexico", *Proceedings of the 11th International*

Offshore and Polar Engineering Conference, Stavanger, Norway.

Yang, C.K. and Kim, M.H. (2011), "The structural safety assessment of a tie-down system on a tension leg platform during hurricane events", *Ocean Syst. Eng*., **1**(4), 263-283.

Yue, B., Campbell, M., Walters, D., Thompson, H. and Raghavan, K. (2010, *Improved SCR design for dynamic vessel application*, OMAE2010-20406.

Zhou, J., Liu, Y. and Li, X. (2010), "Pipe walking-lateral buckling interaction", *Proceedings of Earth and Space 2010: Engineering, Science, Construction, and Operations in Challenging Environment 2010 ASCE*, Hawaii, USA.